Electronic Supplementary Material (ESI) for Journal of Materials Chemistry C.
This journal is © The Royal Society of Chemistry 2023

Supplementary Information

Impacts of PbI_2 on High-Efficiency Perovskite Solar Cells: Exploring Intercalation Orientations and Defects

*Feifei Ren,[a] Huiwen Xiang,[a] Ke Zhao,[b] Chengyan Liu[a]**

[a] Henan Key Laboratory of Photovoltaic Materials, Key Laboratory for Special Functional Materials of Ministry of Education, Henan University, Kaifeng 475004, China

[b] International Laboratory for Quantum Functional Materials of Henan, and School of Physics and Microelectronics, Zhengzhou University, Zhengzhou 450001, China

1. The construction of PbI_2/$CsPbI_3$ heterojunctions

Table S1 The PbI_2//$CsPbI_3$ heterojunctions constructed by the (0 0 1) plane of PbI_2 interfaced with the various low-index planes of $CsPbI_3$, with different surface terminations at the heterointerfaces. The table includes the representations of the heterointerfaces, orientations of lattice vectors, lattice constants and lattice mismatch errors.

Heterointerface	PbI_2		$CsPbI_3$		Lattice matching (Å)	Error (%)	
	$\boldsymbol{a}$ (Å)	$\boldsymbol{b}$ (Å)	$\boldsymbol{u}$ (Å)	$\boldsymbol{v}$ (Å)		$\boldsymbol{a}$:$\boldsymbol{u}$	$\boldsymbol{b}$:$\boldsymbol{v}$
PbI_2(0 0 1)//$CsPbI_3$(1 0 0)	$\sqrt{3}\boldsymbol{a}_0'$ [1 2 0]	$\boldsymbol{a}_0'$ [2 -1 0]	$\boldsymbol{a}_0$ [0 1 0]	$\boldsymbol{a}_0$ [0 0 1]	($3\boldsymbol{a}$, $4\boldsymbol{b}$)//($4\boldsymbol{u}$, $3\boldsymbol{v}$) (24.32, 18.72)//(25.53, 19.15)	4.74	2.25
PbI_2(0 0 1)//$CsPbI_3$(1 1 0)	$\sqrt{3}\boldsymbol{a}_0'$ [1 2 0]	$\boldsymbol{a}_0'$ [2 -1 0]	$\boldsymbol{a}_0$ [0 0 1]	$\sqrt{2}\boldsymbol{a}_0$ [1 -1 0]	($3\boldsymbol{a}$, $2\boldsymbol{b}$)//($4\boldsymbol{u}$, $\boldsymbol{v}$) (24.32, 9.36)//(25.53, 9.03)	4.74	3.77
PbI_2(0 0 1)//$CsPbI_3$(1 3 0)	$\sqrt{3}\boldsymbol{a}_0'$ [1 2 0]	$\boldsymbol{a}_0'$ [2 -1 0]	$\boldsymbol{a}_0$ [0 0 1]	$\sqrt{10}\boldsymbol{a}_0$ [3 -1 0]	($3\boldsymbol{a}$, $4\boldsymbol{b}$)//($4\boldsymbol{u}$, $\boldsymbol{v}$) (24.32, 18.72)//(25.53, 20.19)	4.74	7.28
PbI_2(0 0 1)//$CsPbI_3$(1 1 1)	$\sqrt{3}\boldsymbol{a}_0'$ [1 2 0]	$\boldsymbol{a}_0'$ [2 -1 0]	$\sqrt{6}\boldsymbol{a}_0$ [2 -1 -1]	$\sqrt{2}\boldsymbol{a}_0$ [0 1 -1]	($2\boldsymbol{a}$, $2\boldsymbol{b}$)//($\boldsymbol{u}$, $\boldsymbol{v}$) (16.21, 9.36)//(15.64, 9.03)	3.64	3.65
PbI_2(0 0 1)//$CsPbI_3$(1 1 2)	$\sqrt{3}\boldsymbol{a}_0'$ [1 2 0]	$\boldsymbol{a}_0'$ [2 -1 0]	$\sqrt{3}\boldsymbol{a}_0$ [1 1 -1]	$\sqrt{2}\boldsymbol{a}_0$ [1 -1 0]	($4\boldsymbol{a}$, $2\boldsymbol{b}$)//($3\boldsymbol{u}$, $\boldsymbol{v}$) (32.42, 9.36)//(33.17, 9.03)	2.26	3.65

Table S2 The PbI_2⊥$CsPbI_3$ heterojunctions constructed by the (1 2 0) plane of PbI_2 interfaced with the various low-index planes of $CsPbI_3$, with different surface terminations at the heterointerfaces. The table includes the representations of the heterointerfaces, orientations of lattice vectors, lattice constants and lattice mismatch errors.

Heterointerface	PbI_2		$CsPbI_3$		Lattice matching (Å)	Error (%)	
	$\boldsymbol{a}$ (Å)	$\boldsymbol{b}$ (Å)	$\boldsymbol{u}$ (Å)	$\boldsymbol{v}$ (Å)		$\boldsymbol{a}$:$\boldsymbol{u}$	$\boldsymbol{b}$:$\boldsymbol{v}$
PbI_2(1 2 0)⊥$CsPbI_3$(1 0 0)	$\boldsymbol{a}_0'$ [2 -1 0]	$\boldsymbol{c}_0'$ [0 0 1]	$\boldsymbol{a}_0$ [0 1 0]	$\boldsymbol{a}_0$ [0 0 1]	($4\boldsymbol{a}$, $4\boldsymbol{b}$)⊥($3\boldsymbol{u}$, $5\boldsymbol{v}$) (18.72, 31.58)⊥(19.15, 31.92)	2.30	1.07
PbI_2(1 2 0)⊥$CsPbI_3$(1 1 0)	$\boldsymbol{a}_0'$ [2 -1 0]	$\boldsymbol{c}_0'$ [0 0 1]	$\boldsymbol{a}_0$ [0 0 1]	$\sqrt{2}\boldsymbol{a}_0$ [1 -1 0]	($4\boldsymbol{b}$, $2\boldsymbol{a}$)⊥($5\boldsymbol{u}$, $\boldsymbol{v}$) (31.58, 9.36) ⊥ (31.92, 9.03)	1.07	3.65
PbI_2(1 2 0)⊥$CsPbI_3$(1 3 0)	$\boldsymbol{a}_0'$ [2 -1 0]	$\boldsymbol{c}_0'$ [0 0 1]	$\boldsymbol{a}_0$ [0 0 1]	$\sqrt{10}\boldsymbol{a}_0$ [3 -1 0]	($4\boldsymbol{a}$, $5\boldsymbol{b}$)⊥($3\boldsymbol{u}$, $2\boldsymbol{v}$) (18.72, 39.48)⊥(19.15, 40.38)	2.30	2.20
PbI_2(1 2 0)⊥$CsPbI_3$(1 1 1)	$\boldsymbol{a}_0'$ [2 -1 0]	$\boldsymbol{c}_0'$ [0 0 1]	$\sqrt{6}\boldsymbol{a}_0$ [2 -1 -1]	$\sqrt{2}\boldsymbol{a}_0$ [0 1 -1]	($2\boldsymbol{b}$, $2\boldsymbol{a}$)⊥($\boldsymbol{u}$, $\boldsymbol{v}$) (15.79, 9.36)⊥(15.64, 9.03)	0.96	3.65
PbI_2(1 2 0)⊥$CsPbI_3$(1 1 2)	$\boldsymbol{a}_0'$ [2 -1 0]	$\boldsymbol{c}_0'$ [0 0 1]	$\sqrt{3}\boldsymbol{a}_0$ [1 1 -1]	$\sqrt{2}\boldsymbol{a}_0$ [1 -1 0]	($4\boldsymbol{b}$, $2\boldsymbol{a}$)⊥($3\boldsymbol{u}$, $\boldsymbol{v}$) (31.58, 9.36)⊥(33.17, 9.03)	4.79	3.65

2. Heterojunction structures

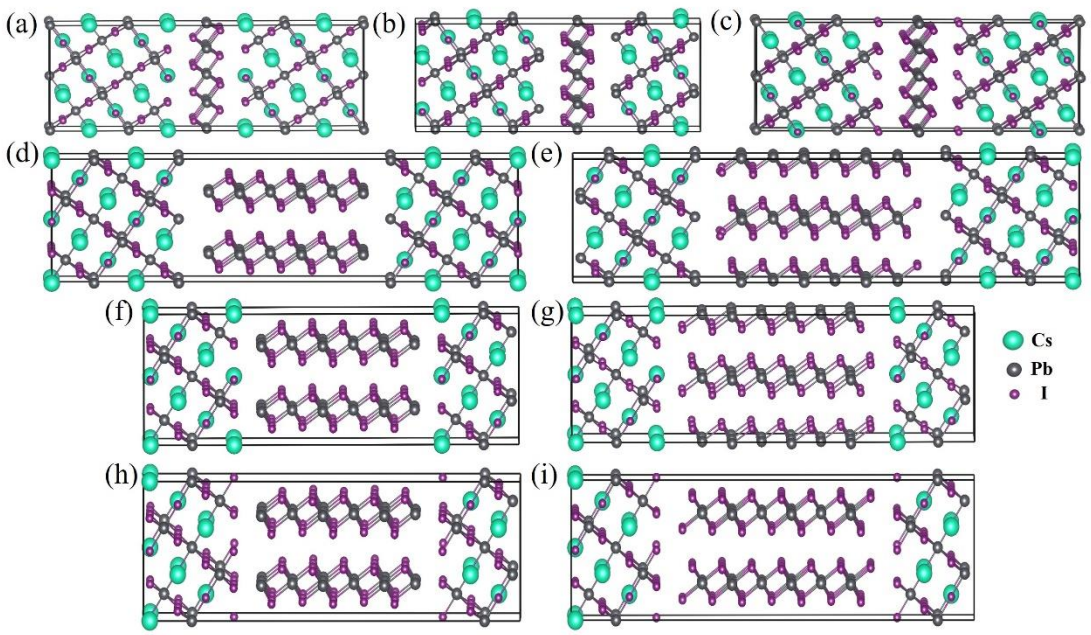

Fig. S1 The initial heterojunctions constructed based on the intercalation orientations of PbI_2 interfaced with the (1 1 1) plane of perovskite with the various surface terminations at heterointerface. (a) PbI_2//$CsPbI_3$-CsI, (b) PbI_2//$CsPbI_3$-I, (c) PbI_2//$CsPbI_3$-Pb, (d) PbI_2-Pb⊥$CsPbI_3$-Pb, (e) PbI_2-I⊥$CsPbI_3$-Pb, (f) PbI_2-Pb⊥$CsPbI_3$-CsI, (g) PbI_2-I⊥$CsPbI_3$-CsI, (h) PbI_2-Pb⊥$CsPbI_3$-I, (i) PbI_2-I⊥$CsPbI_3$-I. The atoms colored by cyan, grey and purple represent Cs, Pb and I, respectively.

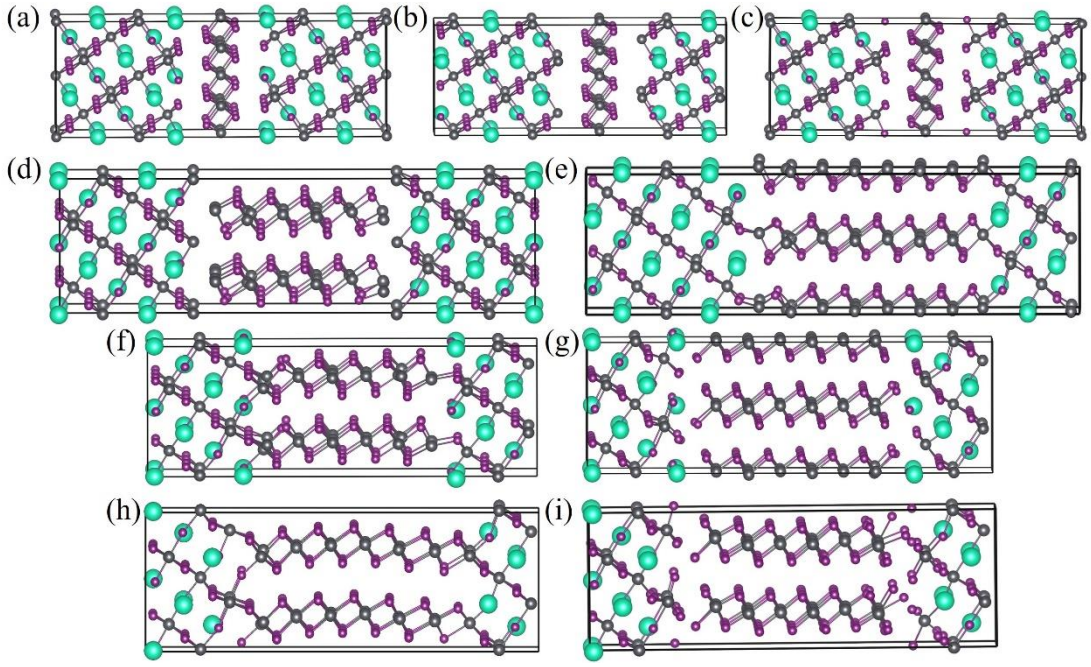

Fig. S2 The relaxed heterojunctions corresponding to those in Figure S1. (a) PbI_2//$CsPbI_3$-CsI, (b) PbI_2//$CsPbI_3$-I, (c) PbI_2//$CsPbI_3$-Pb, (d) PbI_2-Pb⊥$CsPbI_3$-Pb, (e) PbI_2-I⊥$CsPbI_3$-Pb, (f) PbI_2-Pb⊥$CsPbI_3$-CsI, (g) PbI_2-I⊥$CsPbI_3$-CsI, (h) PbI_2-Pb⊥$CsPbI_3$-I, (i) PbI_2-I⊥$CsPbI_3$-I.

3. Band alignment calculations

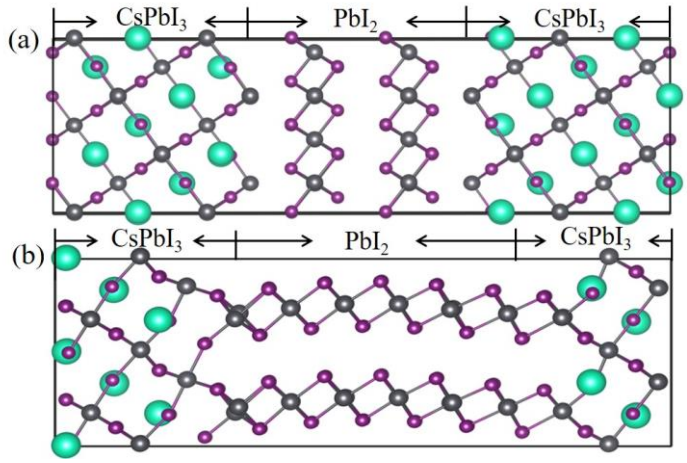

Fig. S3 Atomic structures of (a) PbI_2//$CsPbI_3$-Pb and (b) PbI_2-Pb⊥$CsPbI_3$-I heterojunctions with two layers of PbI_2 parallelly and vertically interfaced with the (1 1 1) plane of $CsPbI_3$, respectively.

The absolute deformation potential (ADP) method is used to calculate the band alignment between $CsPbI_3$ and PbI_2.[S1] The average 1s core level of the iodine atoms that are far away from the interface of heterojunctions is employed as the reference level. The calculation steps are shown schematically in Fig. S4. To obtain the natural valence band offset of $CsPbI_3$ and PbI_2 at their respective equilibrium lattice constants, we firstly calculate the difference in energy separation between the core level and the valence band maximum (VBM) of $CsPbI_3$ and PbI_2 at their averaged volume.

$$\Delta E_{\mathrm{v,\,core}}^{(\mathrm{av})}(\mathrm{PbI_2/CsPbI_3}) = \Delta E_{\mathrm{v,\,c'}}^{(\mathrm{av})}(\mathrm{CsPbI_3}) - \Delta E_{\mathrm{v,\,c}}^{(\mathrm{av})}(\mathrm{PbI_2}) \tag{S1}$$

where $\Delta E_{\mathrm{v,c'}}^{(\mathrm{av})}(\mathrm{CsPbI_3})$ and $\Delta E_{\mathrm{v,c}}^{(\mathrm{av})}(\mathrm{PbI_2})$ represent the energy separation between the core level and VBM of $CsPbI_3$ and PbI_2 at their averaged volume, respectively, by performing separate bulk calculations. To align the reference levels of $CsPbI_3$ and PbI_2, we construct the $(PbI_2)_{16}$//$(CsPbI_3)_{18}$ and $(PbI_2)_{24}$⊥$(CsPbI_3)_{14}$ superlattices at the average lattice constants of the interfaces. The slab thickness is carefully checked with the valence band offset convergence to less than 0.02 eV. The difference of core levels $\Delta E_{\mathrm{C,C'}}^{(\mathrm{av})}$ between PbI_2 and $CsPbI_3$ in each half of the superlattice is derived by

$$\Delta E_{\mathrm{C,C'}}^{(\mathrm{av})}(\mathrm{PbI_2/CsPbI_3}) = E_{\mathrm{C'}}(\mathrm{CsPbI_3}) - E_{\mathrm{C}}(\mathrm{PbI_2}) \tag{S2}$$

Combining with the equations (S1) and (S2), the valance band offset $\Delta E_{\mathrm{v}}^{(\mathrm{av})}$ at their averaged lattice constants is given by

$$\Delta E_{\mathrm{v}}^{(\mathrm{av})}(\mathrm{PbI_2/CsPbI_3}) = \Delta E_{\mathrm{v,core}}^{(\mathrm{av})}(\mathrm{PbI_2/CsPbI_3}) + \Delta E_{\mathrm{C,C'}}^{(\mathrm{av})}(\mathrm{PbI_2/CsPbI_3}) \tag{S3}$$

The volume deformation which is used to accommodate the construction of the heterojunction is accounted for the correction of the valence band. The final natural band alignment ΔE_{v} can be obtained by

$$\Delta E_{\mathrm{v}}(\mathrm{PbI_2/CsPbI_3}) = \Delta E_{\mathrm{v}}^{(\mathrm{av})}(\mathrm{PbI_2/CsPbI_3}) + a_{\mathrm{v}}^{\mathrm{VBM}}(\mathrm{PbI_2})\mathrm{d}\ln V(\mathrm{PbI_2}) + a_{\mathrm{v}}^{\mathrm{VBM}}(\mathrm{CsPbI_3})\mathrm{d}\ln V(\mathrm{CsPbI_3}) \quad \text{(S4)}$$

where $a_{\mathrm{v}}^{\mathrm{VBM}}$ is the change in the VBM under a hydrostatic volume deformation. $\mathrm{d}\ln V = \Delta V / V$ is the relative volume difference between the equilibrium systems of PbI_2 and $CsPbI_3$ and their average.

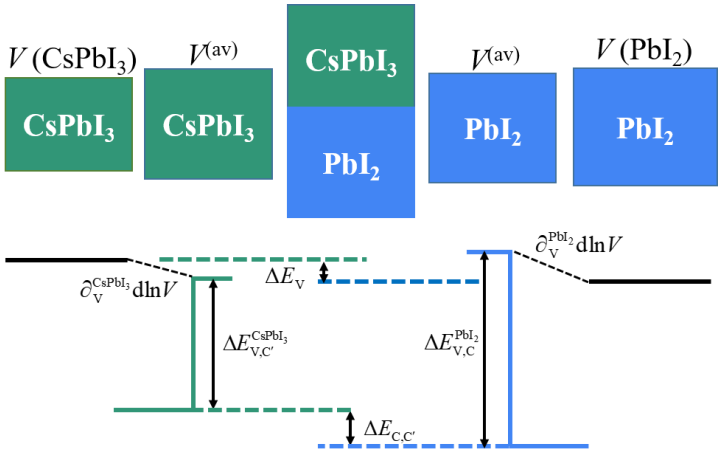

Fig. S4 The schematics for calculations of valence band offset between PbI_2 and $CsPbI_3$.

4. Electronic structures of the pristine heterointerfaces

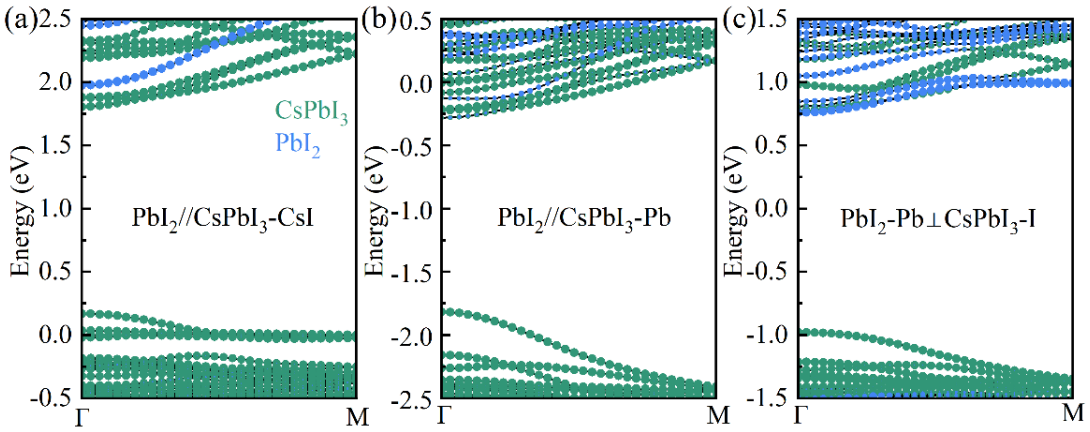

Fig. S5 Band structures of the three energetically favorable heterointerfaces. (a) PbI_2//$CsPbI_3$-CsI, (b) PbI_2//$CsPbI_3$-Pb and (c) PbI_2-Pb⊥$CsPbI_3$-I. The green and blue circles represent the contribution of electronic states from the atoms of the $CsPbI_3$ and PbI_2 systems, respectively. The size of the circles indicates the relative contribution of the corresponding atoms to the energy bands. Fermi energy level is set as the reference zero point.

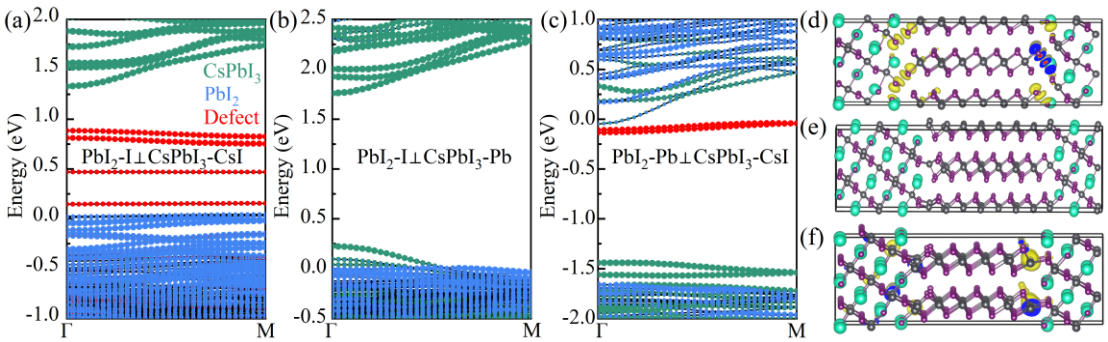

Fig. S6 Band structures and atomic structures. (a)-(c) band structures of PbI_2-I⊥$CsPbI_3$-CsI, PbI_2-I⊥$CsPbI_3$-Pb and PbI_2-Pb⊥$CsPbI_3$-CsI, respectively, whose partial charge densities of the interface are shown in (d)-(f), respectively.

The PbI_2-I⊥$CsPbI_3$-CsI heterointerface exhibits several deep defect levels within the band gap, as shown in Fig. S6(a). These defect levels stem from the antibonding states of I-I at the interface depicted in Fig. S6(d). In contrast, the PbI_2⊥$CsPbI_3$-Pb heterointerface displays no defect states within the band gap due to the complete saturation of I dangling bonds on the Pb-terminated (1 2 0) plane of PbI_2 at the surface termination of $CsPbI_3$. The PbI_2-Pb⊥$CsPbI_3$-CsI heterointerface produces several shallow defect levels near the conduction band minimum (CBM) as a result of unpaired electrons from the Pb atoms at the interface, as shown in Fig. S6(f).

5. Formation energies of the V_I and I_i defects near and far away from the PbI_2-Pb⊥$CsPbI_3$-I heterointerface

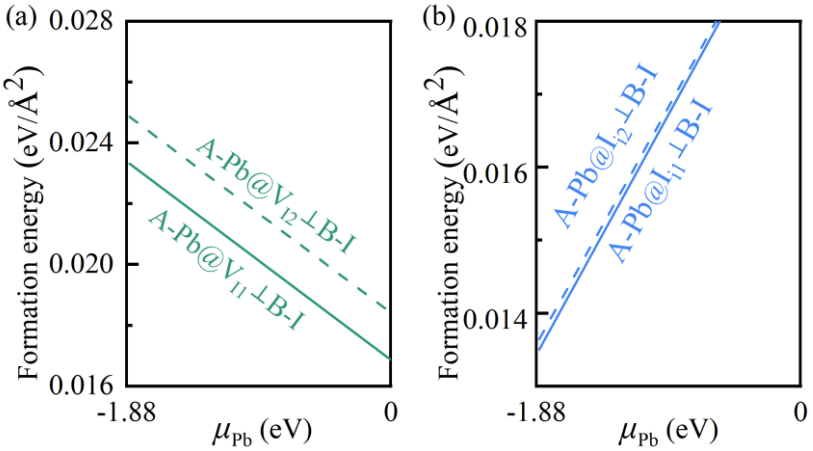

Fig. S7 The interface formation energy of the V_I and I_i defects near (solid lines) and far away (dashed lines) from the PbI_2-Pb⊥$CsPbI_3$-I heterointerface.

6. Electronic and atomic structures of the I and Pb related defects in PbI_2/$CsPbI_3$ heterointerface

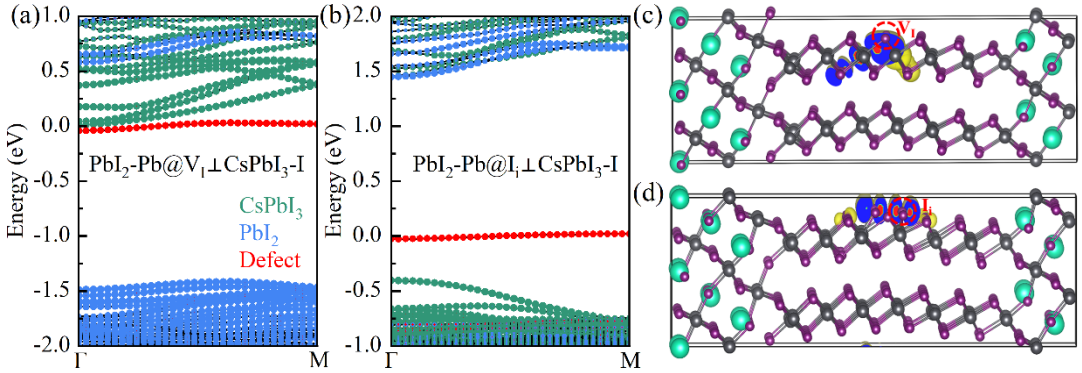

Fig. S8 Band structures and atomic structures of the V_I and I_i defects far away from the PbI_2-Pb⊥$CsPbI_3$-I heterointerface. (a) and (b) The band structures of the PbI_2@V_I⊥$CsPbI_3$-CsI and PbI_2@I_i⊥$CsPbI_3$-CsI heterointerfaces, respectively, whose partial charge densities of defects are shown in (c) and (d).

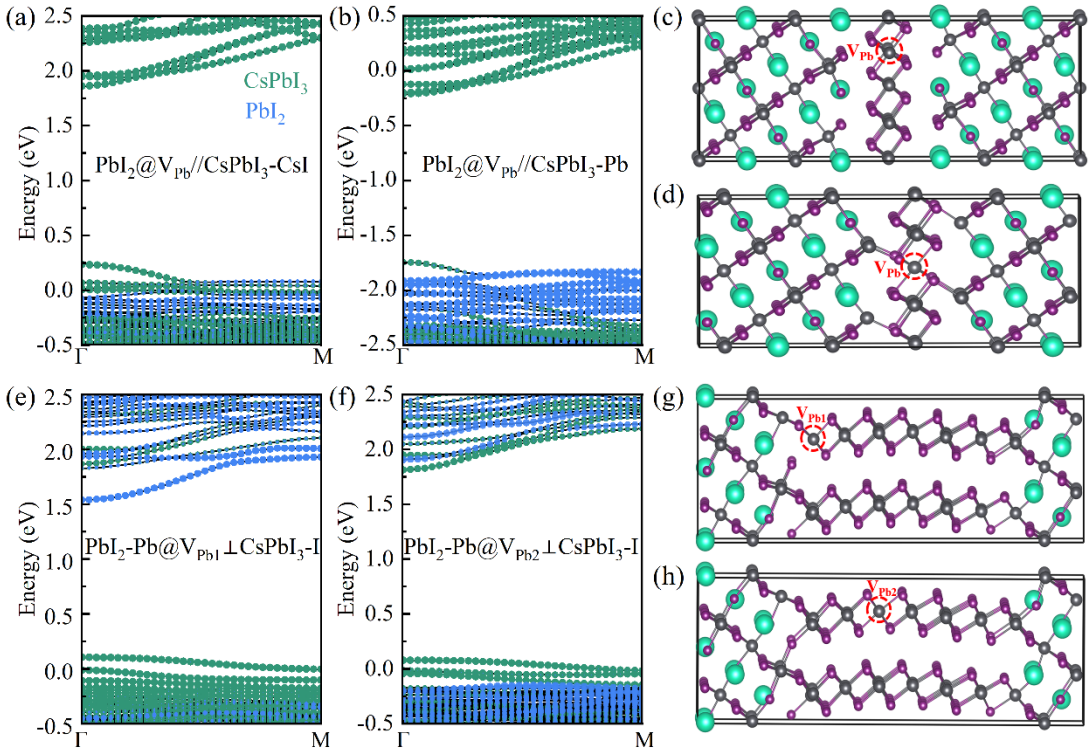

Fig. S9 Band structures and atomic structures of the defective $PbI_2/CsPbI_3$ heterointerfaces with Pb related defect at the layered PbI_2. (a) and (b) The band structures of the $PbI_2@V_{Pb}//CsPbI_3$-CsI and $PbI_2@V_{Pb}//CsPbI_3$-Pb heterointerfaces, respectively, whose atom structures are shown in (c) and (d). (e) and (f) The band structures of the PbI_2-Pb@V_{Pb1}⊥$CsPbI_3$-I and PbI_2-Pb@V_{Pb2}⊥$CsPbI_3$-I heterointerfaces, respectively, whose atom structures are shown in (g) and (h).

7. Band edge energetics and carrier transport

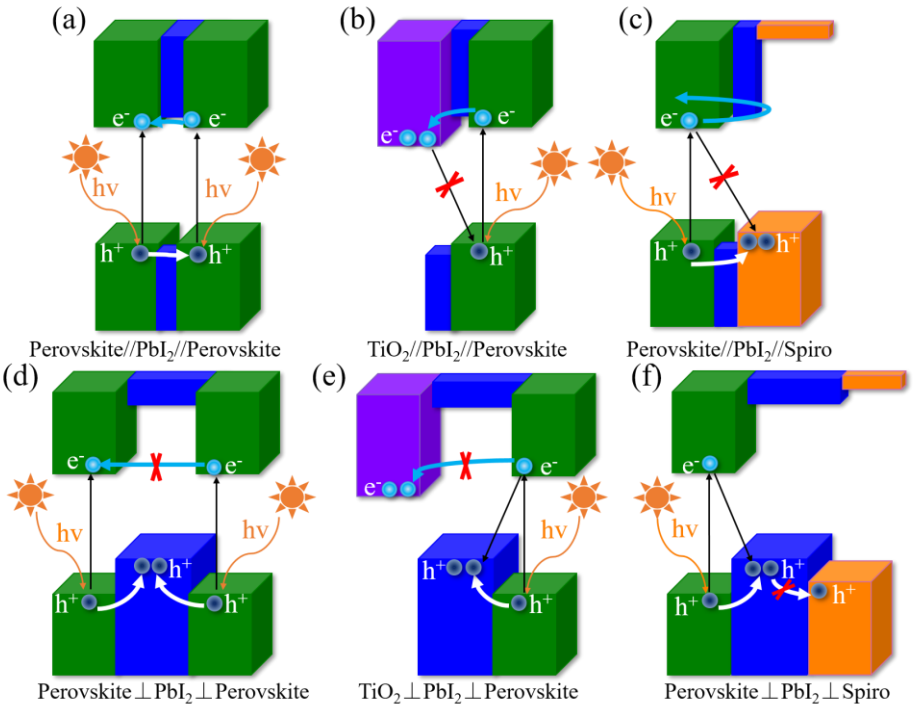

Fig. S10 Schematic diagrams of band edge energetics illustrating the impacts of intercalating orientation of PbI_2 on the carrier transfer of PSC. The band edge positions of TiO_2 (electron transfer layer) and Spiro-OMeTAD (denoted as Spiro, hole transfer layer) relative to those of perovskite are collected from Ref. S2. (a), (b) and (c) show the band alignments of heterojunctions formed by a layered PbI_2 parallelly intercalated into two perovskite grains, between TiO_2 and perovskite, and between perovskite and Spiro, respectively. (d), (e) and (f) show the cases of PbI_2 vertically intercalated into them. The band alignments between perovskite and PbI_2 are shown in Fig. 2 of the main text.

By analyzing the band edge energetics of TiO_2 (electron transfer layer) and Spiro-OMeTAD (denoted as Spiro, hole transfer layer) relative to that of perovskite,[S2] the impacts of the intercalating PbI_2 on carrier transfer in PSC devices are studied. The parallel intercalation of the layered PbI_2 in perovskite grains (perovskite//PbI_2//perovskite) does not subsequently hinder the transfer of the photoexcited electrons and holes in the absorber, due to the slightly higher CBM and lower VBM of PbI_2 than those of perovskite, as shown in Fig. S10(a). To maximize the passivating effect and minimize the hindrance of carrier transfer, PbI_2 should be processed into multiple thin layers, which can be achieved by the post-treatment with the organic ammonium salts.[S3] On the other hand, the parallel intercalation of PbI_2 into the electron transfer interface (TiO_2//PbI_2//perovskite) and the hole transfer interface (perovskite//PbI_2//Spiro) can suppress the interfacial nonradiative recombination as shown in Fig. S10(b) and S10(c). Despite the parallel intercalation of PbI_2, the extraction of carriers is not significantly impeded, as the built-in electric fields at the contact interfaces can derive carriers across the low energy barrier of the thin-layered PbI_2.

The vertical intercalation of the layered PbI_2 into perovskite (perovskite⊥PbI_2⊥perovskite) exhibits a pronounced type-II band alignment as shown in Fig. S10(d). Consequently, both the high barrier height and the great layer thickness impede carrier transfer through the perovskite grains. The PbI_2 at the electron transfer contact interface (TiO_2⊥PbI_2⊥perovskite) seriously hinders electron extraction due to its high CBM as shown in Fig. S10(e). Furthermore, electrons accumulated at the CBM of perovskite can readily recombine with holes at the high VBM of PbI_2. At the hole transfer interface (perovskite⊥PbI_2⊥Spiro), PbI_2 efficiently extracts holes from the absorber but obstructs hole transfer to electrode due to its high VBM, as shown in Fig. S10(f). Therefore, despite its passivation benefits, the vertical intercalation of the layered PbI_2 into PSCs is not a favorable scheme, given the pronounced type-II band alignment and the great layer thickness.

References

S1. Y.-H. Li, A. Walsh, S. Chen, W.-J. Yin, J.-H. Yang, J. Li, J. L. F. Da Silva, X. G. Gong and S. Wei, *Appl. Phys. Lett.*, 2009, **94**, 212109.

S2. S. Akin, Y. Altintas, E. Mutlugun, S. Sonmezoglu, *Nano Energy* 2019, **60**, 557-566.

S3. X. Jiang, J. Zhang, X. Liu, Z. Wang, X. Guo and C. Li, *Angew. Chem. Int. Ed*. 2022, **61**, e202115663.